NEUTRAL COMPOSITION OBTAINED FROM A ROCKET-BORNE MASS SPECTROMETER

Edward J. Schaefer and Myron H. Nichols*
Department of Aeronautical and Astronautical Engineering
The University of Michigan, Ann Arbor, Michigan

Abstract

A quadrupole mass spectrometer has been designed for studies of neutral atmospheric composition between 100 and 200 km using Nike-Cajun and Nike-Apache rockets. A successful technique of ejecting the payload at altitude from an evacuated volume to reduce contaminants has been developed. The ion source has been designed for direct immersion in the ambient atmosphere with the greatest open-look angle possible. The number of surface collisions experienced by a particle prior to ionization has thereby been reduced to the order of one or two and the probability of surface recombination of atomic oxygen has been correspondingly reduced to the order of one percent.

The first successful daytime flight of a continuing program yielded an O_1/O_2 current ratio which was unity at 118 km and 3.1 at 134 km. Preliminary data analysis of the first successful nighttime flight yielded O_1/O_2 current ratios in substantial agreement with the daytime flight and extended the data to 190 km where the ratio was 9.5. These values are about an order of magnitude greater than those obtained heretofore by other investigators and achieve much closer agreement with ultra-violet measurements, and theoretical predictions.

On the basis of the daytime data, a mean molecular weight of approximately 24.6 is derived at 134.5 km.

Introduction

In the latter part of 1958, a research group at The University of Michigan undertook to develop an instrumentation for measuring the ambient neutral composition. The chief objective was to design a mass spectrometer which would reduce the probability of surface recombination of atomic oxygen to a negligible value. In this manner, it was anticipated that flight measurements of atomic oxygen would be in closer agreement with theory [1] and with values obtained from ultra-violet absorption measurements [2] than have been obtained by earlier mass spectrometer measurements [3,4]. In addition, techniques to achieve negligible errors due to chemical reactions at the filament and out-gassing of the rocket were to be developed.

A secondary objective was to design the experiment for use aboard a small vehicle such as the Nike-Cajun (or, more recently, the Nike-Apache) so that a time and latitude survey would be ultimately possible.

Two successful flight tests of the instrumentation have been accomplished to date. Both have yielded O_1/O_2 current ratios approximately an order of magnitude greater than obtained by former mass spectrometer measurements.

Part I of this paper gives a detailed description of the techniques and instrumentation employed in these measurements. Experimental results of the daytime flight are presented in detail. Part II presents preliminary data from the nighttime flight.

The work performed on this program has been generously supported by the National Aeronautics and Space Administration.

PART I

1. INSTRUMENTATION

After a review of the types of mass spectrometers and ion sources suitable for the mass number range 4 to 46 and adaptable for use on small rockets, the mass spectrometer first described by Paul, Reinhardt, and von Zahn [5] was chosen. A complete description of this spectrometer as adapted for rocket use is given in Appendix A of this paper. Figure 1-1 is a line schematic of the mass spectrometer. As evident from the photographs in Appendix A, the ion source is directly exposed to the ambient atmosphere there being no inlet tubes or enclosing walls. The design of the "open" ion source is made possible by a property of the Paul spectrometer by which the indicated ion mass is independent of the axial ion velocity in the analyzer. Only the percentage transmission and the resolution are dependent on ion velocity. The maximum ion velocity is determined by the potential of the grid G in Fig. 1-1 which serves the dual function of accelerating the ionizing electrons from filament F and providing the electric field gradient to accelerate the positive ions toward the ground plane C and inlet port I. The grid G is operated between 45 and 50 volts which, in conjunction with the other design parameters, provides the desired resolution (see Appendix A). The total area of the analyzing chamber breather holes, 1.3 cm^2, as compared with the area of the inlet port, 5.1×10^{-3} cm^2, insures that only a negligible fraction of the gas in the analyzer is returned to the ion source. This, together with the open ion source, guarantees that each ambient atom or molecule experiences, on the average, the order of one surface collision prior to ionization. After ionization, a collision with any surface will result in loss of the ion. An attendant feature of the ion source is essentially zero time constant in reaching equilibrium with the environment.

In order to eliminate the possibility of contamination from gases trapped in the rocket and adsorbed

*Now at San Diego State College, San Diego, Calif.

on its surfaces, the entire instrumentation is enclosed in a capsule which is ejected from an evacuated container when altitude is reached. Use of "o" rings limits the vacuum in the container to about 1-10μ of pressure.* It may be of interest to note that the capsule is always in the vicinity of room temperature (300°K). It is separated from rocket parts heated by aerodynamic effects prior to initiation of data analysis.

As explained in Appendix A, the mass spectrometer is operated during flight in two alternate modes. One mode yields the usual spectral peaks and the other mode, called the "staircase" mode, yields essentially the integral of the peak spectrum. These two modes are illustrated in Fig. A-5 of Appendix A. From Fig. A-2 (and checked by Fig. A-5) of Appendix A it is evident that the mass number scale for the peak spectrum must be multiplied by approximately 9/7 to give the mass number scale for the staircase mode. Both modes are useful in interpreting the data. For example, the staircase mode gives the total residual ion current due to ions whose masses lie above the mass range of the instrument. When approaching the sensitivity limit of the instrument where the mass peaks tend to be lost "in the noise" their presence is revealed by the staircase mode and a more precise result can be obtained. At increasingly high pressures, due to scattering collisions, sensitivity reaches a maximum then decreases and the staircase degenerates into a curve rather than a series of steps whereas the spectral peaks show no significant change in shape. Thus the staircase mode identifies the branch of the double-valued curve upon which the instrument is operating. Finally, the staircase mode assures 100% transmission and therefore serves as a calibration of the major peaks.

Prior to flight, laboratory calibrations were run on the entire instrumentation using air. A high speed vacuum system was used in connection with an adjustable leak in order to minimize the effect of adsorption on the walls of the system and interaction with the hot filament electron source until the ultimate vacuum was approached. Figures 1-2 and 1-3 serve to illustrate the results of preflight laboratory calibrations which were made by first increasing the pressure from the ultimate and then decreasing the pressure. The fork in the O_2/N_2 current ratio at low pressures (Fig. 1-2) is probably due to the greater affinity of O_2 for the chamber walls which operates to deplete it on the increasing pressure cycle and enrich it due to desorption on the decreasing pressure cycle.** The apparent enrichment of argon at low pressures (Fig. 1-3) as evidenced by the A/N_2 current ratio is probably due to the nature of the leak. Both O_2 and A show apparent enrichment at higher pressures due to scattering collisions and their smaller cross-section as compared with N_2. In both cases it will be noted the staircase yields the more accurate ratio at high pressures because of the stronger focusing action in this mode of operation.

As evident in Fig. 1-2, these preflight calibrations yielded an O_1^+/O_2 current ratio of about 0.04. This result indicates that the average electron energy was less than 45 volts due to space charge effects around the fine wires of the accelerating grid. The basis for this conclusion is given in Section 3. The N_1/N_2 current ratio was about 0.015.

2. DAYTIME FLIGHT DATA

The instrumentation described in the previous section was flown on Nike-Cajun rocket NASA 10.91 UA from Wallops Island, Va. (latitude 37°50'N, longitude 75°29'W) at 1302 EST, 18 May 1962. The apogee was 134.5 km and the horizontal velocity at apogee was approximately 800 ft/sec. The spin period was 1.2 sec and the precession period was 31 sec.

To provide the reader with some feeling for the quality of the data, Figs. 2-1a and b are composite photographs of unretouched telemetered conventional and staircase spectra at 120 km altitude upleg and at 133 km upleg. Figures 2-2a, b, c, d, and e show raw, uncorrected ion current as a function of altitude for total current, N_2, O_2, O_1, and A. Figures 2-3a, b, and c show the number densities in the ion source for N_2, O_2 and A as obtained from the raw data by means of laboratory calibrations.***

Figure 2-4 shows the ratio of O_1 ion current to O_2 ion current. The interpretation of this ratio in terms of number densities requires a knowledge of the relative ionization cross sections of O_1 and O_2. The results for the minor constituents are given in Appendix B.

3. CORRECTION FOR RELATIVE IONIZATION CROSS-SECTIONS FOR O_1 AND O_2

Since no means for generating neutral O_1 atoms were available to us for laboratory calibration, it is necessary to use published data on the O_1 ionization cross section. Also, as already mentioned, we are uncertain as to the effective energy of the ionizing electrons because of space charge effects in the neighbor-

*In the case of the daytime flight (Nike-Cajun NASA 10.91 UA), the procedure was modified by first evacuating the container and then filling with helium to one atmosphere of pressure. A pop-out diaphragm permitted release of the helium on the upleg portion of the trajectory.

**As part of the mass spectrometer development, calibration curves were run on N_2 and O_2 separately, using the adjustable leak procedure. On the basis of these calibrations, the predicted ratio of O_2 ion current to N_2 ion current for ground air is 0.14.

***In obtaining these curves, only data above 106 km on the upleg and above 100 km on the downleg were used. Lower altitude data were not used because the density in the analyzing section was high enough to affect the ion currents by scattering collisions as evidenced by a rounded shape of the staircase spectrum. The densities in the analyzing section and ion source could be substantially different in flight because of aerodynamic effects. Hence, calibration results, obtained at a uniform density could be applied only where peak spectral current values are functions of processes in the ion source only.

hood of the fine wires constituting the electron accelerating grid.

Data on ionization cross-section of O_2 and O_1 have been published by Fite and Brackmann [6]. For 45 electron volts, the data indicate a relative O_1/O_2 cross-section ratio of approximately 0.85. However, since the laboratory calibrations showed 4% O_1 ions, the data of [6] indicate that the effective energy was in the neighborhood of 25-30 electron volts. At this energy, the experimental data of Fite and Brackmann indicate that the ratio of the O_1 cross-section to the O_2 cross-section is nearly unity although the theory indicates a ratio of approximately 0.5. In the data interpretation in this paper, an ionization cross-section ratio of unity will be assumed. Under this assumption, Figure 2-4 also gives the ratio of number densities of O_1 to O_2 in the ion source.

4. INTERPRETATION OF THE DATA—DYNAMIC EFFECTS

In interpreting the data, the motion of the instrument package, must be taken into account. In flight number NASA 10.91 UA the horizontal velocity at apogee was approximately 800 ft/sec. In this flight there was a precession period of approximately 31 sec which gave a pronounced modulation to the data, particularly on the downleg.

It is the purpose of this section to discuss effects of dynamics on the interpretation of the results. Precise quantitative analysis is prohibitively complicated in view of the involved geometry of the ion source and the nature of the interactions between the impinging atoms and molecules and the atoms of the base metal with an adsorbed gas layer. A recent review of the data on thermal accommodation coefficients [7] discusses the defects in existing data. Hurlbut [7] reports data on scattering angle but velocity distributions are not available. Thus, there is considerable uncertainty in the quantitative effects of surface interaction. For purposes of illustration and estimation, idealized models and calculations are presented with the object of roughly bounding the effect.

For purposes of discussion, assume that the ion source consists of a flat plate containing the inlet port to the analyzer. Assume also that the grid structure, filament, etc. (see Fig. 1-1), consisting of very fine wires presents a total surface area so small that the probability of a particle colliding with them is negligible. Assume further that the velocity vector of the package is parallel to the analyzer axis. Finally, assume that the ambient mean free path is large compared to the dimensions of the ion source. Now, if the ambient particles are perfectly reflected from the plate (specular reflection, no energy loss) with no recombination, the presence of the plate and the velocity of the package would have no effect on the ratios of the ion currents of the various constituents.

This follows from the equation

$$n_i v_i = -n_r v_r \tag{4-1}$$

where: n_i = number density of incident particles in the ion source
n_r = number density of reflected particles in the ion source
v_i = incident velocity normal to plate
v_r = reflected velocity normal to plate.

Because of the assumption of perfect reflection, $v_i = -v_r$. Hence $n_i = n_r$, independent of the type of particle.

The foregoing idealized model is never realized in practice because the metal atoms (and the adsorbed gas particles) are not infinitely massive in relation to the atmospheric constituents. It serves, however, to place a lower limit on the correction to convert concentration ratios in the ion source to ambient conditions. An upper limit may be derived by assuming that the collisions between the impinging particles and the individual surface atoms are elastic and that the lines of the centers of the colliding particles are parallel to V, the velocity of the package. Then, neglecting the thermal energy of the surface atoms,

$$v_r = v_i(R-1)/(R+1) \tag{4-2}$$

where: $R = m/M$
m = mass of gas atom or molecule
M = mass of surface atom.

Then Eq. (4-1) becomes

$$n_r/n_i = -v_i/v_r = (1+R)/(1-R) \tag{4-3}$$

For numerical illustration, assume that the surface is stainless steel with M = 56, and that the incident particles are O_2 with m = 32. Then

$$(n_r/n_i)_{O_2} = 3.7 \tag{4-4}$$

and for O_1

$$(n_r/n_i)_{O_1} = 1.8 \tag{4-5}$$

Assuming that the package velocity V is much larger than the thermal velocities, this process leads to an enrichment of O_2 over O_1 by the factor E_ℓ where

$$E_\ell = (1+3.7)/(1+1.8) = 1.7 \tag{4-6}$$

When V is of the order of the thermal velocity of the metal atoms or less, a thermal interaction model with an appropriate accommodation coefficient may be a better approximation. For example, assuming a Maxwellian distribution for the atmospheric constituents, the number of particles striking the plate per sq cm/sec is given by

$$n_p = n_i\left\{(kT/2\pi m)^{1/2}\exp(-mV^2/2kT) + [V/(2\pi)^{1/2}]\int_{-\infty}^{V(m/kT)^{1/2}}\exp(-t^2/2)\,dt\right\} \quad (4\text{-}7)$$

where: k = Boltzmann's constant

T = ambient temperature in °K.

Assuming T = 300°K, and using the horizontal velocity at apogee of V = 800 ft/sec = 2.44×10^4 cm/sec,

$$(n_p)_{O_2} = 2.74 \times 10^4 (n_i)_{O_2} \text{ molecules/sq cm/sec}$$

and

$$(n_p)_{O_1} = 3.04 \times 10^4 (n_i)_{O_1} \text{ molecules/sq cm/sec} \quad (4\text{-}8)$$

Now assuming that all atoms and molecules striking the metal surface reach thermal equilibrium with the surface before leaving it, the density of reflected particles $n_r/2$ is given by the equation

$$n_p = n_r \int_0^\infty u\,p(u)\,du \quad (4\text{-}9)$$

where p(u) is the velocity distribution of the particles and where u is the velocity normal to the plate. Assuming a Maxwellian distribution and a metal temperature of 300°K,

$$(n_r)_{O_2} = 2.5(n_i)_{O_2}$$

$$(n_r)_{O_1} = 1.9(n_i)_{O_1} \quad (4\text{-}10)$$

In this case the enrichment factor E_t for O_2 over O_1 calculates to be

$$E_t = (0.805+1.25)/(0.728+0.95) = 1.2 \quad (4\text{-}11)$$

From Fig. 2-2a it appears that the package was flying with the analyzer axis closest to the velocity vector at apogee inasmuch as apogee time is intermediate between two minima in total ion current. We may thus infer that the enrichment factor lies somewhere between 1.0 for perfect reflection and 1.7 for elastic collisions.

From the ion current data, it is clear that the minima in the up and down curves are all spaced closely to 31 sec apart. This can be explained by precession as indicated schematically in Fig. 4-1. The precession cone half angle is estimated in Appendix D to be 44°. The higher O_1/O_2 ratios which occur in the minima of ion current in the downleg as seen in Fig. 2-4 can be explained by the higher thermal velocity of O_1 relative to O_2. This enables relatively more O_1 atoms than O_2 molecules to reach the ionizing region in the ion source at angles of attack greater than 90°.

In interpreting the data it is important to note that the minima of the upleg data at 108 km, 125 km, and 133 km, approximately, and the maxima of the downleg data at 127 km and 110 km fall closely to a single smooth curve. On the basis of Fig. 4-1, this may be explained by the hypothesis that the instrumentation is flying more closely to right angles to the trajectory at these points. On this basis, it may be postulated that the data most closely relate to ambient conditions at these points.

It is also important to note from Fig. 2-4 that between 108 km and 117 km and also in the neighborhood of 128 km (above which there is sufficient spread in the data to obscure the effect) the O_1/O_2 upleg ion current ratios are nearly identical to the downleg. Based on Fig. 4-1, the authors roughly estimate the angle of attack at 108 km on the upleg at about 55° and at 113 km on the downleg at about 105°. Since these angles are quite different and yet the O_1/O_2 ion current ratios are nearly the same, one is led to the hypothesis that the interaction with the metal surfaces is closer to perfect reflection than thermalization or elastic collision with the individual surface atoms. However, it should be pointed out that the rather large ring at the top of the ion source, which can be seen clearly in Fig. A-4 of Appendix A, can interact with the gas flow, that the precession half-angle of 44° is only approximate, and that we have no direct knowledge of the attitude of the instrumentation during the flight. In future flights, the surface area of the ring will be substantially reduced.

5. MEAN MOLECULAR WEIGHT

From the ion source particle concentration data (Figs. 2-3a, b, and c) Table 5.1 can be constructed. The number density for O_1 is obtained from the number density of O_2 multiplied by the O_1/O_2 ion current ratio (Fig. 2-4), assuming negligible surface recombination (Appendix C) and equal ionization cross sections as stated in Section 3.

Table 5-1

Number Densities in the Ion Source at Apogee (134.5 km)

Constituent	Particles/cm³
N_2	8.2×10^{10}
O_2	1.1×10^{10}
O_1	3.4×10^{10}
A	$\sim 0.04 \times 10^{10}$

The mean molecular weight at any altitude is given by

$$\overline{M} = \sum_{j=1}^{k} n_j M_j \Big/ \sum_{j=1}^{k} n_j \qquad (5\text{-}1)$$

where n_j is the number density of the jth component and M_j is its molecular weight. In order to determine the ambient number density from the data, a correction factor for surface interaction effects must be applied. Assuming the elastic collision model with instrumentation velocity V large compared to ambient thermal velocities, the correction factor C_j to be applied to the ion source number density of the jth component to obtain its ambient number density is, from Eq. (4-3),

$$C_j = \frac{1}{2}(1-R_j)$$

Letting the surface be iron (M = 56), Table 5-2 can be constructed

Table 5-2

Correction Factors for Elastic Collision Model

M_j	R_j	C_j
16	0.286	0.36
28	0.500	0.25
32	0.571	0.21
40	0.715	0.14

Using these correction factors and the data at apogee, the "corrected" mean molecular weight $\overline{M}_\ell$ for 134.5 km calculates to be, for the lower bounding value:

$$\overline{M}_\ell = 24.1 \qquad (5\text{-}2)$$

For true specular reflection with no loss of energy, Eq. (4-1) shows that the ratios of the various constituents are the same as they exist in the ambient state. Hence the correction factor C_j is the same for all components and the upper bounding value then becomes

$$\overline{M} = 25.1 \qquad (5\text{-}3)$$

The true value appears to lie somewhere between these two values.

It is interesting to note that the value of 24.4 given in the 1956 ARDC model atmosphere at 135 km is in much better agreement with these data than the value of 28.5 given in the 1959 ARDC model atmosphere.

On the basis of the discussion at the end of the previous section, points at current minima on the upleg and current maxima on the downleg may be most closely representative of the ambient. Mean molecular weights at these points have been computed as before and are plotted in Fig. 5-1.

Based on previous statements, the authors feel that the specular reflection model is a closer representation of conditions in the ion source at these points than the elastic collision model.

6. COMPARISON OF RESULTS

a. Dissociation of Oxygen

Figure 6-1 compares our results with those of Meadows and Townsend [3] and Pokhunkov [8]. The results of [3] were taken from the data of Aerobee-Hi NN 3.19F fired from Fort Churchill, Manitoba, Canada, at 1207 CST on 23 March 1958. Although the O_1/O_2 current ratio is not plotted in [3], the curve in Fig. 6-1 was obtained by dividing the values of the O_1 currents by the O_2 currents contained therein. As discussed in Section 1, the lower ratio obtained by the other investigators may be attributed to surface recombination in the apparatus.

b. O_2 Number Densities

Figure 6-2 compares our results with those of Byram, Chubb and Friedman [2] and of Hinteregger [9]. In this figure our data are uncorrected for dynamic effects. The correction, from Section 4, is bounded between unity and 4.7. (At apogee, calculation based on Eq. (4-10) gives approximately a factor of 2.1 for complete thermalization of incident particles.)

c. Separation Ratio of Argon and Nitrogen

Figure 6-3 compares our results with those of Meadows and Smith [10] in terms of a separation ratio, r,

defined as ion current ratio at altitude* divided by the current ratio from ground air calibration. For reference purposes, the dotted curve is the separation ratio computed for isothermal diffusive equilibrium taken from Figure 6 of Meadows and Townsend [3].

Figure 6-4 compares our results with those of Pokhunkov [4] on the basis of A/N_2 current ratios at altitude.

At this time we have no theory for the difference in the character of our results for the separation ratio and those of the others shown. (We note that the time constant of our ion source in reaching equilibrium with the ambient atmosphere is essentially zero.)

PART II

7. GENERAL

Nike-Apache rocket NASA 14.08 UA was launched from Wallops Island, Virginia, at 0255 EST, 28 March 1963. Apogee was 190 km. While the instrumentation flown on this rocket differed in detail of construction, the design principles remained the same as described in Part I. The only major exception was that the instrumentation of NASA 14.08 UA was flown in an evacuated volume and the helium filling employed on NASA 10.91 UA was abandoned.

8. INSTRUMENTATION

The massenfilter rods for this flight were increased in length from 5 to 7 in. (12.7 to 17.8 cm). A change in the rectifier circuitry provided improved tracking of the rectified DC voltage with the AC sweep voltage. The DC to AC ratio (see Appendix A) was adjusted to a value somewhat higher than that used in the flight of NASA 10.91 UA. These changes improved the resolution of the spectra over the entire sweep range. The quality of the data is illustrated by Figs. 8-1a and b which are composite photographs of unretouched telemetered spectra taken at 131 km and 165 km on the upleg. The mass numbers and probable chemical identifications of the peaks are indicated on the figures. Comparison with Figs. 2-1a and b will show that not only was the resolution improved, but the noise current was substantially reduced. Overall sensitivity in terms of volts at the electrometer output as a function of particle concentration in the ion source was increased by a factor of about 3. The sweep period was increased from 0.5 to 1 sec.

9. DATA RESULTS

Reduction of the data is still in process, hence comments on the results of this flight must be considered to be of a preliminary nature. Figure 9-1 is a plot of a few selected points of the O_1/O_2 ion current ratio obtained on this flight up to 190 km. Also plotted on this figure are a few points obtained from the daytime rocket described in the previous section. At 190 km, the O_2 ion currents were small and hence subject to reading errors. The bars attached to the points in the vicinity of apogee give an indication of the estimated errors. Notwithstanding the error (about 20%) one can safely conclude the O_1/O_2 ion current ratio at apogee is nearly 10. In the overlapping range of data, upleg points of the latter flight agree fairly well with the data of the prior flight. Scatter on the 14.08 UA downleg points is evident in Fig. 9-1 but sufficient detail on probable angles of attack are not available at this writing to offer any further comments.

A quick look at the N_1/N_2 current ratios obtained on this flight indicates that the value lay between 0.02 and 0.04. No comparison with laboratory calibrations has been made as yet, but the authors are drawn to the conclusion that N_1 exists in an amount which is less than 5% of N_2 in the altitude range covered by either flight.

A complete analysis of Nike-Apache flight 14.08 UA will be the subject of a future paper.

ACKNOWLEDGMENTS

The authors are indebted to L. M Jones for his encouragement and assistance throughout the program. Others who made this paper possible are N. J. Wenk and W. H. Hansen for the mechanical designs; C. H. Thornton and E. A. Wenzel for the electronic circuitry and H. F. Henry for the construction of the ion sources. The authors are indebted to J. Brown for his assistance in preparing the figures for this paper as well as his many contributions in research. Many helpful discussions with P. Hays are gratefully acknowledged.

The research described herein was made possible by the support of the National Aeronautics and Space Administration. M. Dubin and Mrs. E. B. Meadows-Reed have provided many stimulating discussions in the field of upper atmosphere research.

*Corrected for dynamic effects relative to their instrument.

REFERENCES

1. M. Nicolet. Physics of the Upper Atmosphere. Academic Press, New York and London (1960). Ed. J. A. Ratcliffe, 29-35.
2. E. T. Byram, T. A. Chubb, and H. Friedman. Dissociation of Oxygen in the Upper Atmosphere. Phys. Rev. 98 (1955), 1594-1597 (Fig. 4 abscissa are 1 km low as later corrected by authors).
3. E. B. Meadows and J. W. Townsend, Jr. IGY Rocket Measurements of Arctic Atmospheric Composition Above 100 km. Proc. First Int. Space Sci. Symp., Nice (1960). Ed. H. K. Kallmann Bijl (North-Holland, Amsterdam), 175-198.
4. A. A. Pokhunkov. Mass Spectrometer Investigation of the Structural Parameters of the Earth's Atmosphere at Altitudes from 100 to 210 km. Planet Space Sci. 9 (1962), 269-279. Trans. from Iskusstvennye Spntniki Zemli 7 (1961), 89-100.
5. W. Paul, H. P. Reinhard, and V. von Zahn. Das Elektrische Massenfilter als Massenspektrometer und Isotopentrenner. Zeitschrift fur Physik, 152 (1958), 143-182.
6. W. L. Fite and R. T. Brackman. Ionization of Atomic Oxygen on Electron Impact. Phys. Rev. 113 (1959), 815.
7. F. C. Hurlbut. Studies of Molecular Scattering at the Solid Surface. J. Appl. Phys. 28, 844-850.
8. A. A. Pokhunkov. The Study of Upper Atmosphere Neutral Composition at Altitudes Above 100 km. Proc. First Int. Space Sci. Symp., Nice (1960). Ed. H. K. Kallmann Bijl (North-Holland, Amsterdam), 101-106.
9. H. E. Hinteregger. Absorption Spectrometric Analysis of the Upper Atmosphere in the EUV Region. J. Atmos. Sci. 19 (1962), 351-368.
10. E. Meadows-Reed and C. R. Smith. Mass Spectrometric Investigations of the Atmosphere Between 100 and 227 km Over Wallops Island, Va. NASA Tech. Note TND 1851.

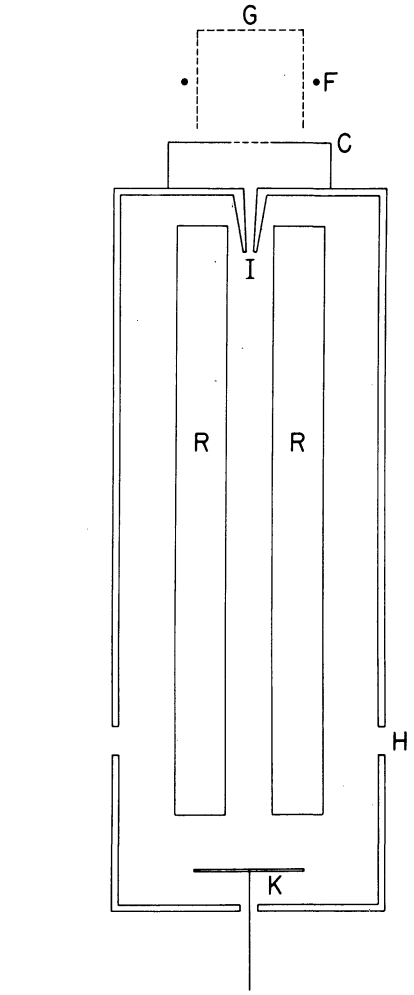

Fig. 1-1. Mass spectrometer line schematic.

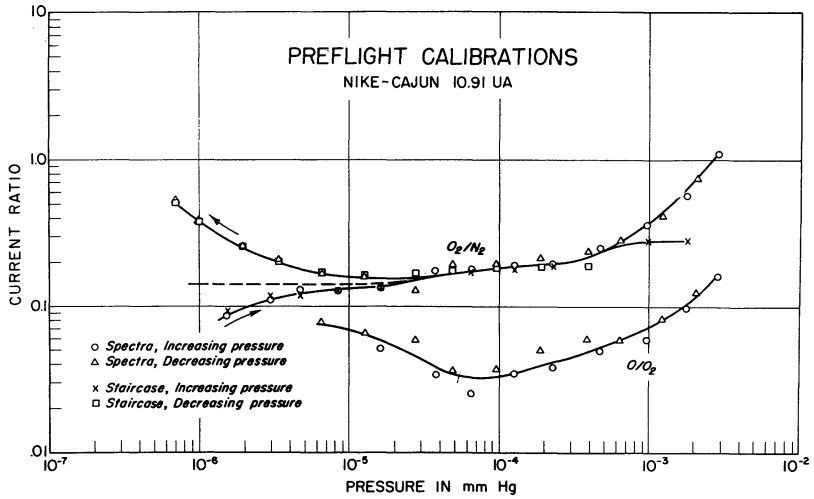

Fig. 1-2. Preflight calibrations.

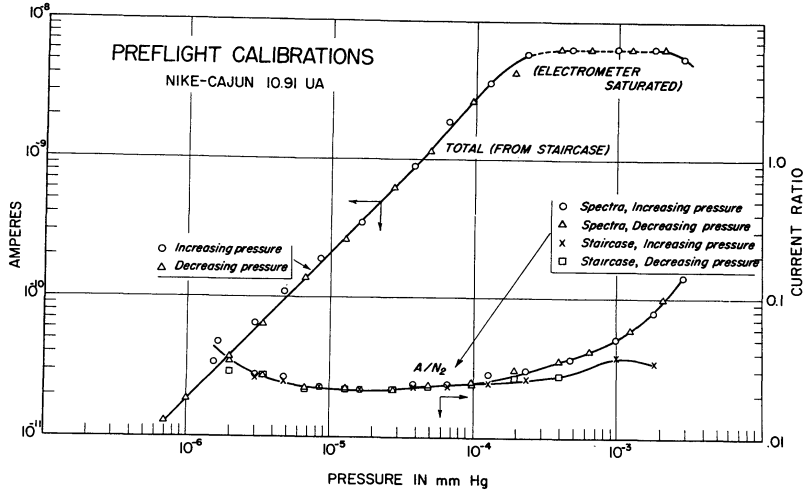

Fig. 1-3. Preflight calibrations.

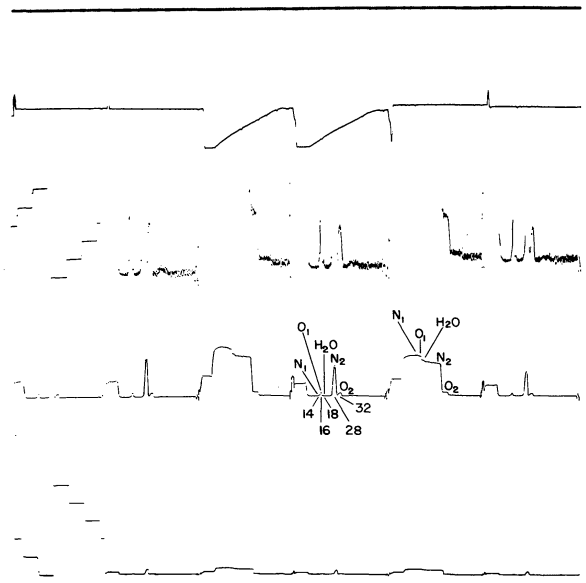

NIKE-CAJUN-1091 UA---120KM - UPLEG-124SEC

(a)

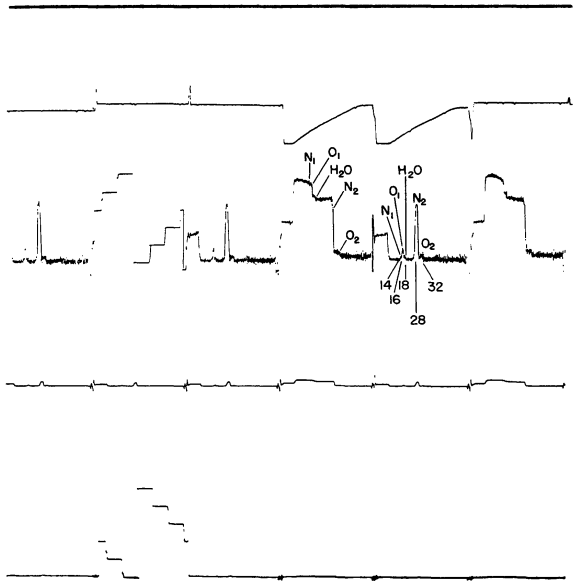

NIKE-CAJUN-1091 UA---133KM - UPLEG-163SEC

(b)

Fig. 2-1. Composite spectra—daytime.

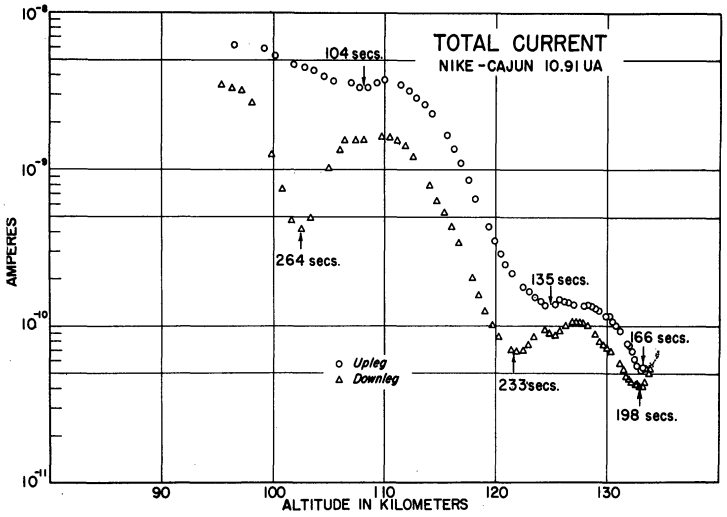

(a)

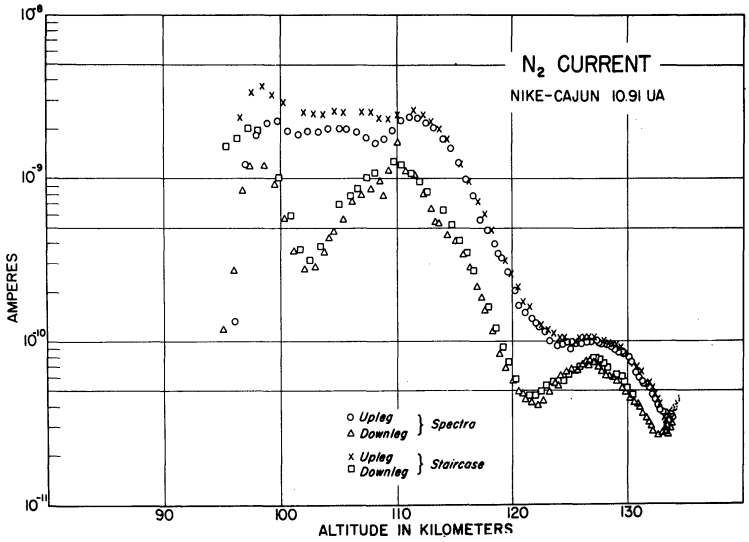

(b)

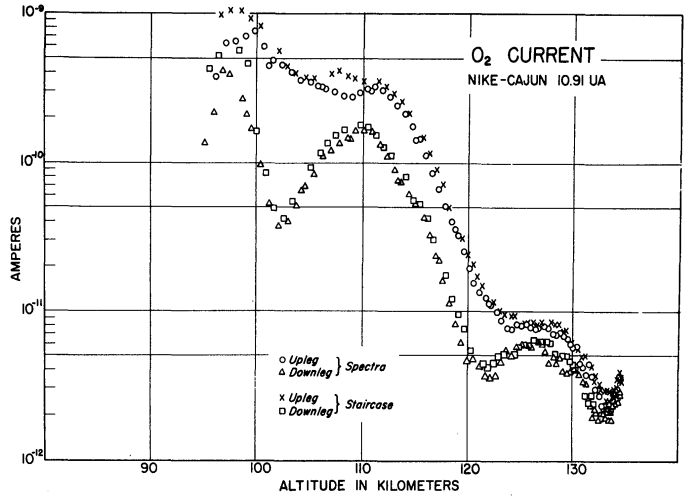

(c)

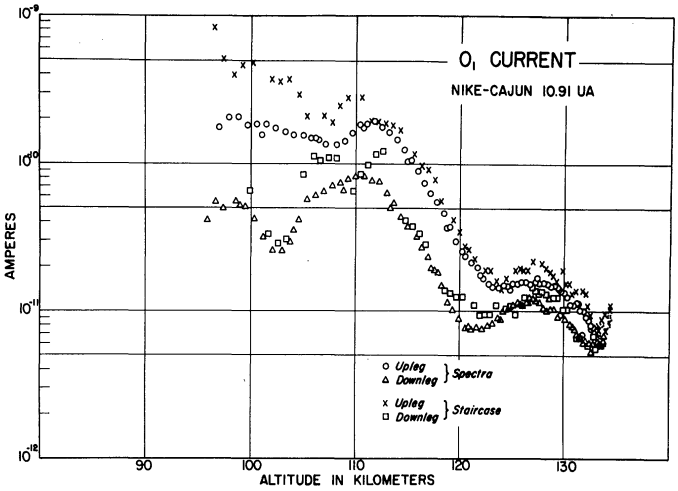

(d)

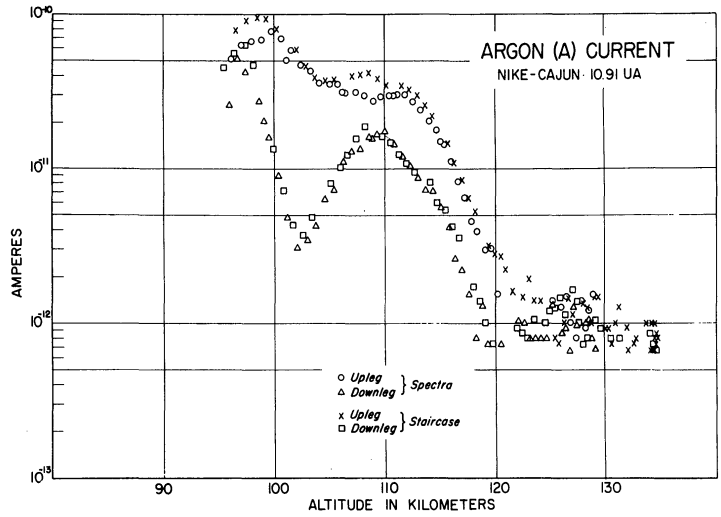

(e)

Fig. 2-2. Flight raw data.

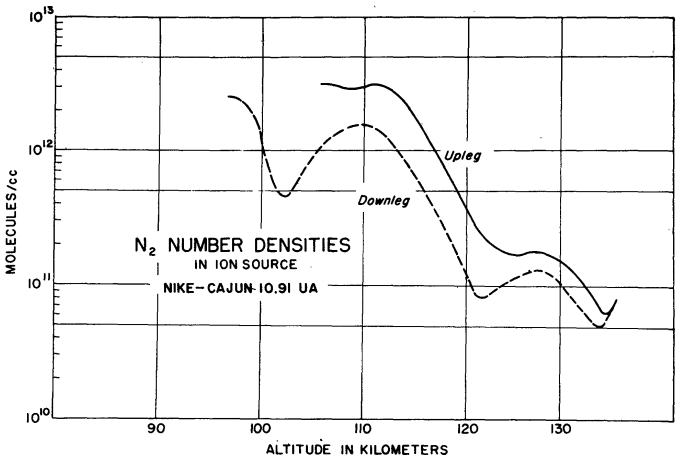

(a)

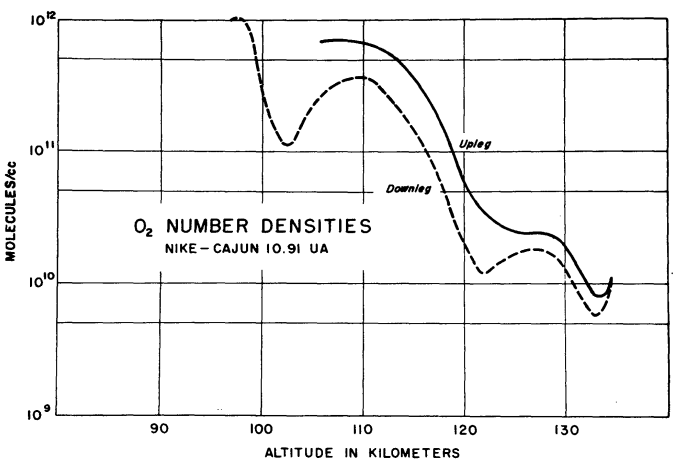

(b)

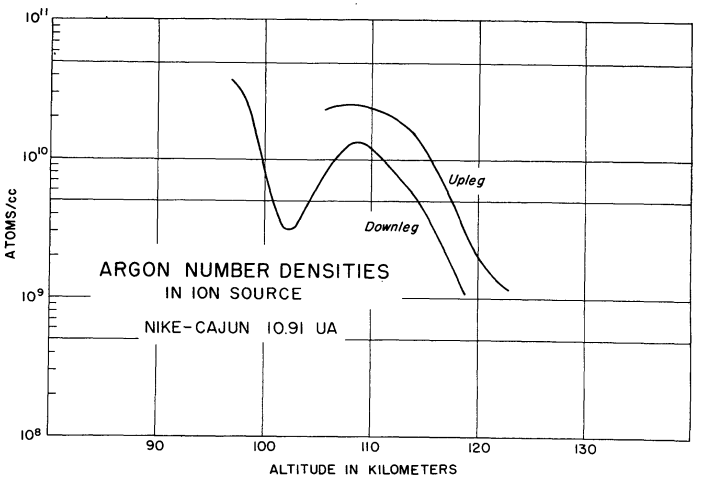

(c)

Fig. 2-3. Computed concentrations.

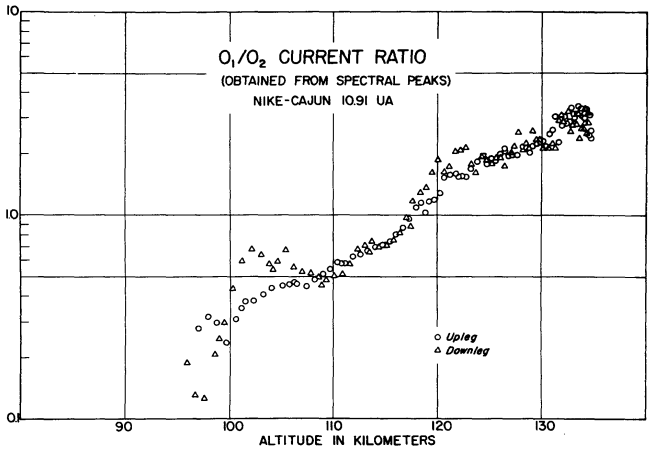

Fig. 2-4. O_1/O_2 current ratio.

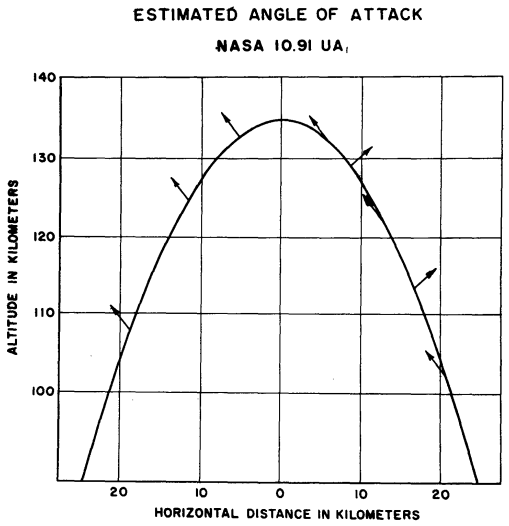

Fig. 4-1. Estimated angle of attack.

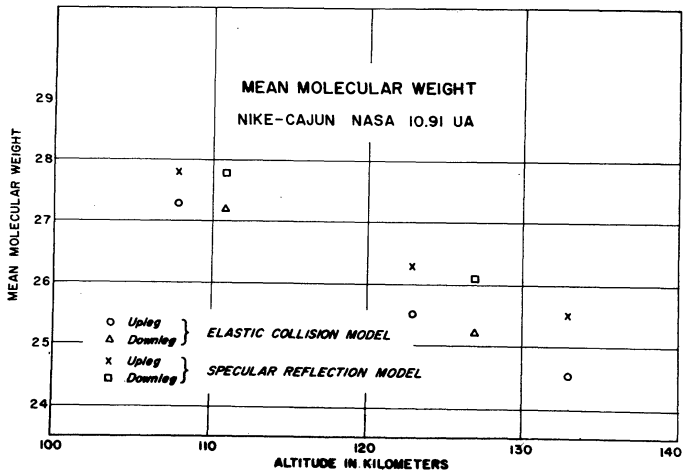

Fig. 5-1. Mean molecular weight.

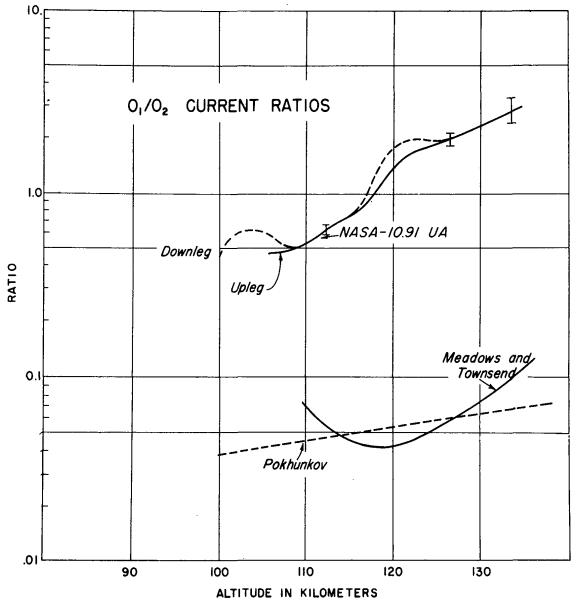

Fig. 6-1. O_1/O_2 current ratios.

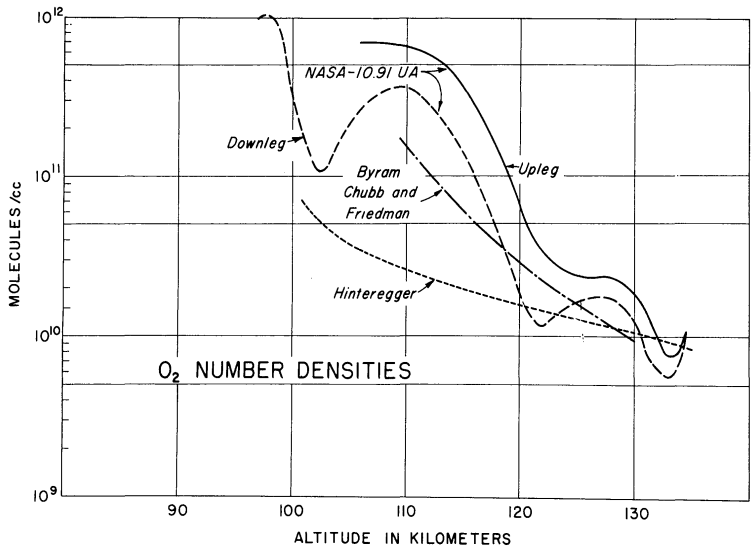

Fig. 6-2. O_2 number densities.

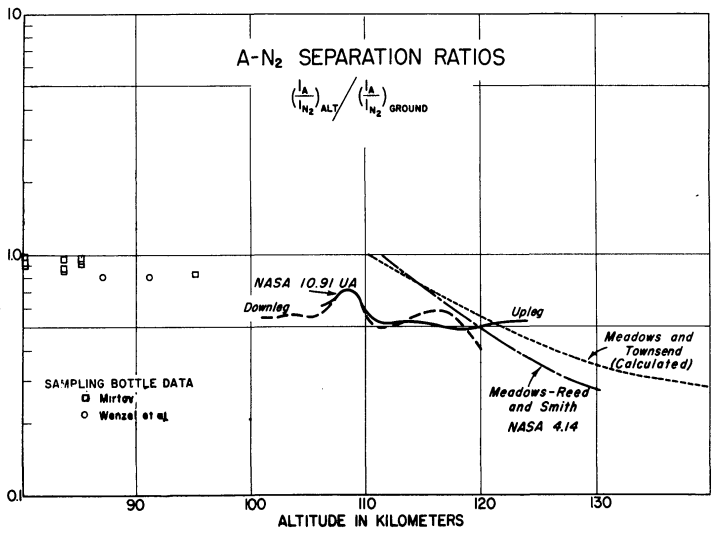

Fig. 6-3. A/N_2 separation ratios.

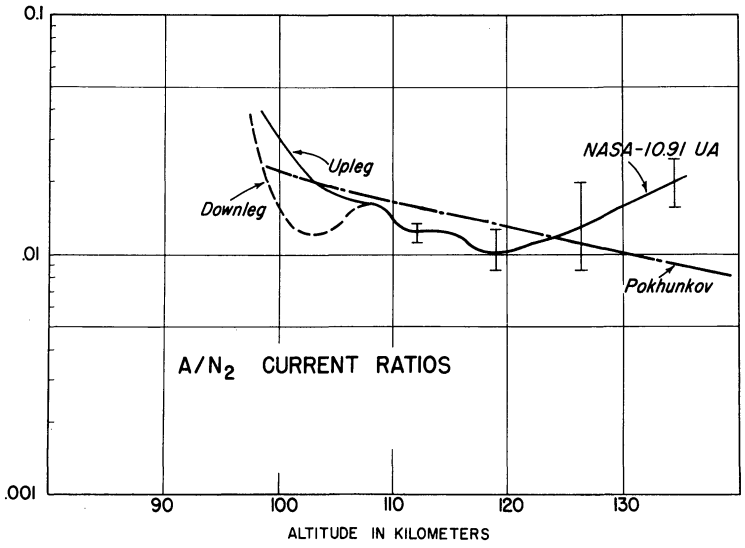

Fig. 6-4. A/N_2 current ratios.

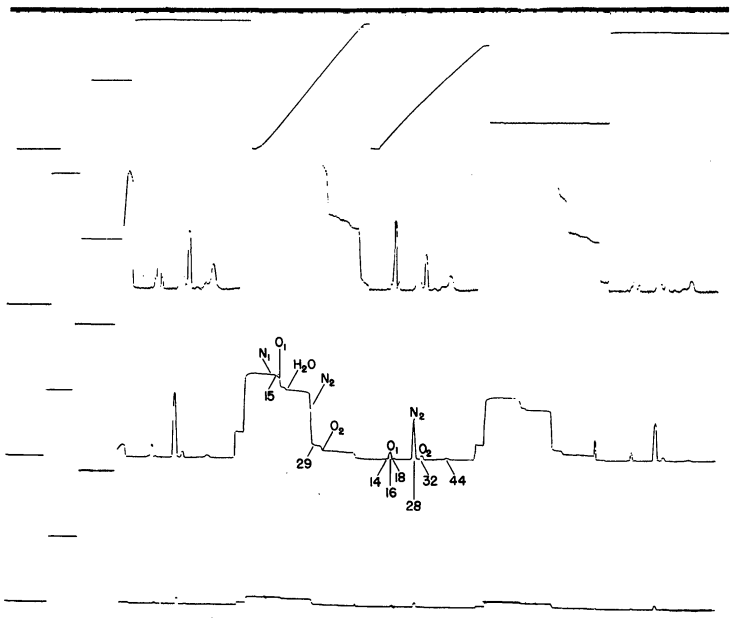

NIKE-APACHE-1408 UA---131 KM -UPLEG- 107 SEC

(a)

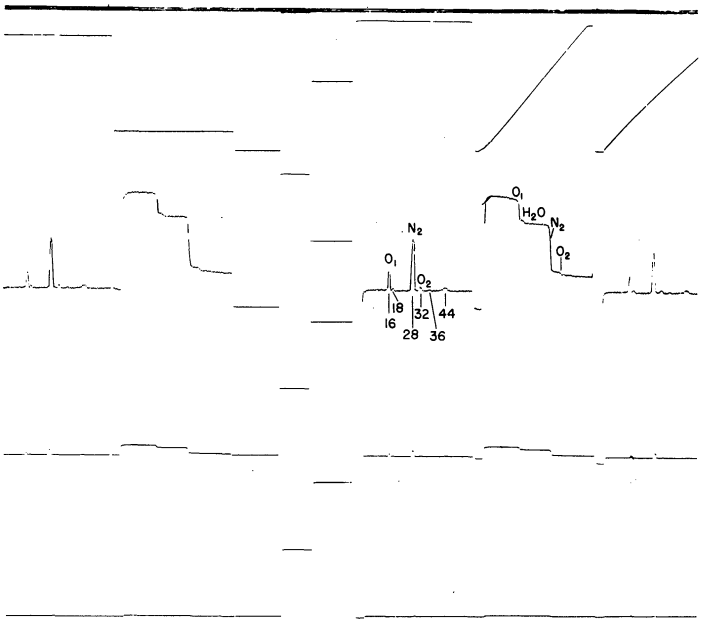

NIKE-APACHE-1408 UA---165 KM -UPLEG- 147 SEC

(b)

Fig. 8-1. Composite spectra—nighttime.

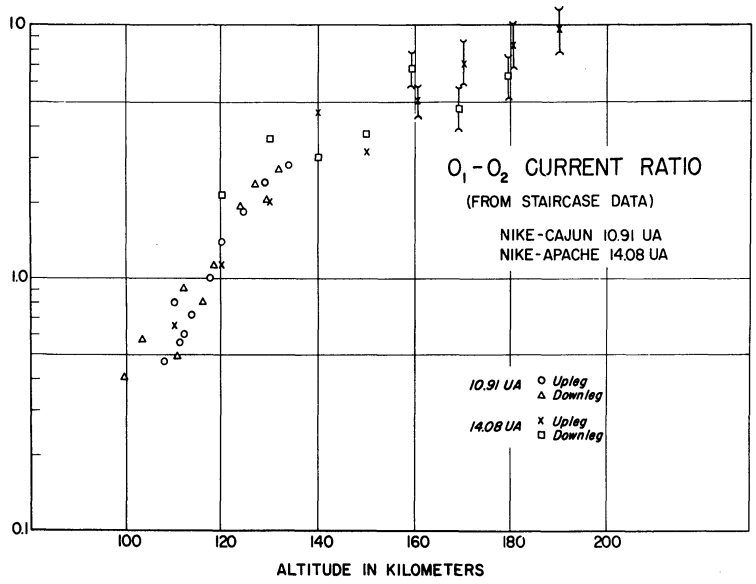

Fig. 9-1. O_1/O_2 current ratio.

APPENDIX A
MASS SPECTROMETER FOR UPPER AIR MEASUREMENTS[1]

E. J. Schaefer[2] and M. H. Nichols,[3] The University of Michigan, Ann Arbor, Michigan

The need for synoptic measurements of atmospheric composition as a function of altitude, latitude and time is becoming increasingly critical. Above about 100 km variations in composition are known to exist. Diffusive separation of the lighter gases modifies composition with altitude. Dissociation of molecular oxygen by the sun's radiation results in variations with time, altitude, and latitude. Recombination processes yield oxides of nitrogen which further modify composition (1-3).[4]

The problem has been investigated by a variety of methods (4-6). Techniques have varied from postflight analysis of upper air samples to mass spectrometer in-flight measurements. The available data thus far, however, must be greatly extended to satisfy the requirements. In particular, variations with altitude, time, and latitude must be investigated on a synoptic basis.

This paper describes the development of an instrumentation package with which to accomplish a synoptic investigation. Support for the work has been furnished by NASA.

MASS SPECTROMETER

The instrument which was selected for in-flight composition analysis is a mass spectrometer first described by Paul, Reinhard, and von Zahn (7). Briefly, its principle of operation is as follows:

The analyzing section of the massenfilter, also known as the Paul tube and quadrupole mass filter, consists of four circular rods positioned 90° apart and connected as shown in Figure A-1. The applied potentials are given by the equations

$$V_{0x} = U + V \cos \omega t \tag{A-1}$$

$$V_{0y} = - V_{0x} \tag{A-2}$$

where V is the peak value of an RF sine wave upon which is superimposed the d-c voltage U. Ideally the rods have a hyperbolic cross section, in which case the potential at any point in the field is given by

$$V_{x,y} = (U + V \cos \omega t)\frac{x^2 - y^2}{R_0^2} \tag{A-3}$$

In practice circular rods of radius 1.16 R_0 closely approximate the ideal field out to about 0.8 R_0.

The equations of motion of a singly charged ion in such a field are

$$m\ddot{x} + 2e(U + V \cos \omega t)x/R_0^2 = 0 \tag{A-4}$$

$$m\ddot{y} - 2e(U + V \cos \omega t)y/R_0^2 = 0 \tag{A-5}$$

Making the substitutions

$$p = \omega t/2 \tag{A-6}$$

$$a = 8eU/mR_0^2\omega^2 \tag{A-7}$$

$$q = 4eV/mR_0^2\omega^2 \tag{A-8}$$

Equations A-4 and A-5 become

$$d^2x/dp^2 + (a + 2q \cos 2p)x = 0 \tag{A-9}$$

$$d^2y/dp^2 - (a + 2q \cos 2p)y = 0 \tag{A-10}$$

These are Mathieu differential equations. Their solutions in terms of a and q yield regions wherein the ionic trajectories are stable and regions where they are unstable. A stable trajectory is defined as one which remains finite in amplitude as p grows infinite. For an ion to be stable in both axes, Equations A-9 and A-10 must each yield a stable solution. The values of a and q in which this condition occurs are given in Figure A-2. From Equations A-7 and A-8

$$a/q = 2U/V \tag{A-11}$$

Thus if the ratio of d-c to RF voltages is held constant, a/q plots as a straight line on Figure A-2. This line is the locus of the working points of all ions. Heavy ions plot close to the origin, and lighter ions plot progressively toward the upper right. If the voltages are increased from zero, the working points will move away from the origin. The lightest ion passes through the stable region first, followed by the heavy ions in order of their mass. Ideally, if a stream of ions is injected at one end of the field, unstable ions are removed by collision with the rods. Stable ions negotiate the length of the field and are detected when they deliver their charge to a collector placed at the other end. In practice, however, there is a minimum number of cycles of the applied RF voltage for which an unstable ion must remain in the field to insure removal. Further, initial conditions of radial velocity and displacement must be restricted to insure collection of a stable ion. Both restrictions increase in severity with resolution. A complete discussion of inlet conditions is beyond the scope of this paper. One appears in (7).

From Figure A-2 it will be noted that if U, and therefore a, is made zero, the locus of all working points lies on the q-axis. At low RF voltages, all ions are in the stable region. As the RF voltage is increased, the working points move away from the origin so that the ions become unstable in order of increasing mass. This mode of operation and the conventional method each offer their own unique advantage. Both are employed in the application described herein.

The massenfilter was selected for upper atmosphere measurements because of the following advantages:

1. It requires no magnetic field; hence it is inherently light in weight.
2. Its construction is simple and rugged.
3. Initial conditions affect only percentage transmission and resolution. They have no effect on the indicated mass of the ion.

---

[1]Abstracted from ARS Journal Vol. 31 No. 12, December, 1961, pp. 1773 to 1776 with minor revisions which incorporate recent developments.

[2]Research Engineer, Department of Aeronautical and Astronautical Engineering.

[3]Professor of Aeronautical and Astronautical Engineering; now at San Diego State College, San Diego, Calif.

[4]Numbers in parentheses indicate References at end of paper.

4. Supporting circuitry is simple. A constant voltage ratio is maintained by rectifying a portion of the RF voltage to obtain the d-c voltage.
5. A linear mass spectrum is obtained from a linear voltage sweep.

FLIGHT DESIGN

For design purposes, four parameters may be independently selected. These, in turn, fix the remainer of the design. The parameters which were selected were resolution, peak RF voltage, rod length, and ion injection voltage. Resolution is here defined as the mass of the ion divided by the width, expressed in mass units, of its spectral peak at half amplitude. A resolution of 40 for mass 46 was considered adequate to separate the gases that can reasonably be expected in the upper atmosphere. Due to the shorter residence times of the lighter ions, resolution will become less as mass is reduced, but less resolution is required as mass decreases. The peak RF voltage was selected to be 500 v as conveniently obtainable in a miniaturized flight package. Rod length was set at 5 in. (12.75 cm) as a reasonable size for small rocket borne experiments. Finally, an injection ion energy of 45 v was selected as a compromise between a low ion velocity that reduces RF power requirements and a high ionic energy that avoids the difficulties inherent in controlling low energy particles. The important design parameters are:

Quantity	Symbol	Value
Mass number	A	46 amu
Resolution	$m/\Delta m$	40
Peak RF voltage	V	500 v
Length of field	L	12.75 cm
Ion injection voltage	V_{in}	45 v
Frequency	f	2.39 Mc
Field radius	R_0	0.522 cm
Rod radius	R_{rod}	0.609 cm
Injection port diameter	D_{in}	0.081 cm
Maximum injection angle	θ	5.25°

A laboratory model is shown in Figure A-3. The collector is positioned with respect to the rods and ion source when assembled into the vacuum container seen in the picture. A completely assembled flight model is seen in Figure A-4. With the exception of insulators, the rhenium filament, and platinum grid, stainless steel is used throughout its construction. An analysis of a calibrated air leak is seen in Figure A-5. Here, the "staircase" sweep illustrates the type of response obtained when the d-c voltage is zero and the working points lie along the q-axis of Figure A-2. In flight use, the type of spectrum is alternated. Complete transmission is assured in the zero d-c sweep. Hence the height of the major steps serves as a calibration of the heights of the corresponding peaks. The conventional spectrum provides a sensitive method of detecting the rarer species. Resolution of the nitrogen peak as a function of ion accelerating voltage is presented in Figure A-6.

INSTRUMENTATION

Perhaps the largest uncertainty in past measurements is the error in analysis due to recombination of atomic oxygen on the walls of the gage. Another uncertainty is the contribution of occluded gases on the rocket to the analysis.

Contamination by rocket gases is avoided by ejecting the entire pressurized instrument package from an evacuated volume when altitude is reached. A sketch of the separation technique is shown in Figure A-7. Emerging from a vacuum, the surface of the instrumentation cylinder is clean of occluded gases. Use of "O" rings limits the attainable vacuum to approximately 1 μ of pressure. A continuing goal is to develop techniques to maintain harder vacuums in a system of this type. (The dipole antenna of Figure A-7 has been replaced by the loop antenna seen in Figure A-8.)

Recombination is minimized by an ion source composed of fine grid structure directly immersed in the ambient gas. This increases the probability that an ambient molecule will enter the ionization volume without first encountering a solid surface where recombination can occur. Future design will attempt to realize an efficient ion source farther removed from the head end of the canister to further reduce the probability of surface recombination.

Figure A-8 is a photograph of instrumentation flown in March, 1963. The massenfilter is at the forward end followed by the electrometer amplifier to detect ion currents. The next chassis is the RF oscillator and rectifier which supplies the rod potentials. Below this is the emission regulator chassis. Following this is a section which provides the oscillator modulated sweep voltage, a periodic in-flight calibration, and commutates the input to the monitor channel in order to telemeter selected voltages throughout the package in sequence. Next is a chassis which delays filament power for 1-1/2 seconds after canister ejection and automatically selects one of two emission current levels according to the sensitivity required. Batteries providing the electronics 28-volt power are next in line followed by a telemeter deck containing the 250 mw transmitter and four subcarrier oscillators devoted to four channels of signal information. Finally, at the bottom of the pressurized section, is the battery pack which provides filament power and a mechanical timer, actuated by take off acceleration, which controls ejection of the canister at altitude. Below the pressurized section, the transmitting loop antenna can be seen in Figure A-8.

ACKNOWLEDGEMENTS

We wish to acknowledge the able assistance of our colleague, D. R. Glass, in the development of the flight massenfilter. J. Brown and E. A. Wenzel made valuable contributions in the development of the flight equipment.

REFERENCES

1. Chapman, S., "The Earth in the Sun's Atmosphere," Scien. Amer., vol. 201, no.4, October, 1959, pp. 64-71.
2. Nicolet, M., "High Atmosphere Densities," Science vol. 127, no. 3310, June 1958, pp. 1317-1320.
3. Nicolet, M., "Atmospheric Models and Thermospheric Gradients," Proc. Fourth Meeting of COSPAR, Florence, Italy, April, 1961 (to be published).
4. Meadows, E. B. and Townsend, J. W., "IGY Rocket Measurements of Arctic Atmospheric Composition Above 100 Km," Space Research, Proc. First Int. Space Science Symp. COSPAR, 1960, pp. 175-198.
5. Pukhunov, A. A., ibid, p. 101.

6. Wenzel, E. A., Loh, L. T., Nichols, M. H. and Jones, L. M., "The Measurement of Diffusive Separation in the Upper Atmosphere," Annals of the IGY, Vol. 12, Part 1, 1960, pp. 407-421.
7. Paul, W., Reinhard, H. P. and von Zahn, U., "Das Elektrische Massenfilter als Massenspektrometer und Isotopentrenner," Zeitschrift fur Physik, vol. 152, 1958, pp. 143-182.

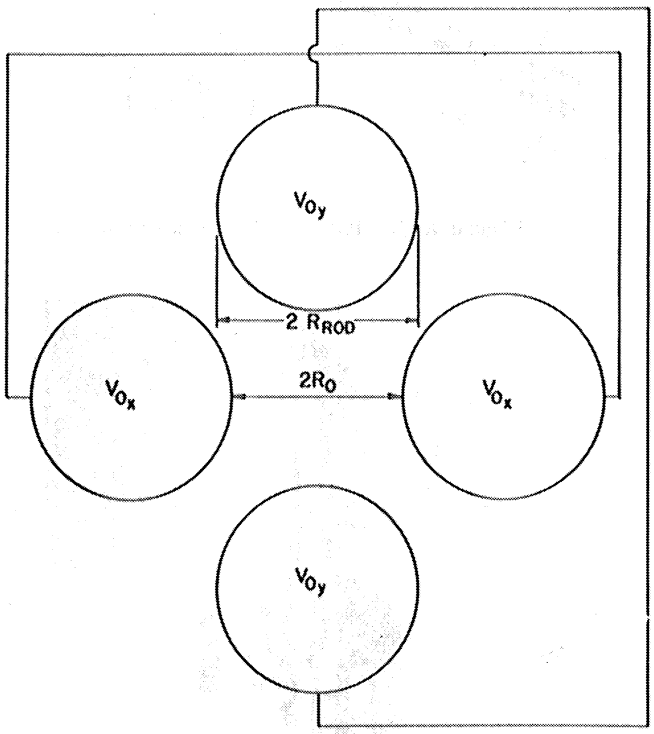

Figure A-1. Circular electrode arrangement.

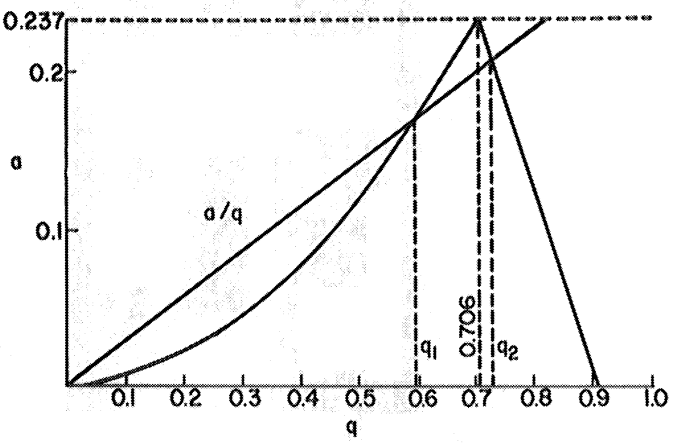

Figure A-2. Massenfilter stability diagram.

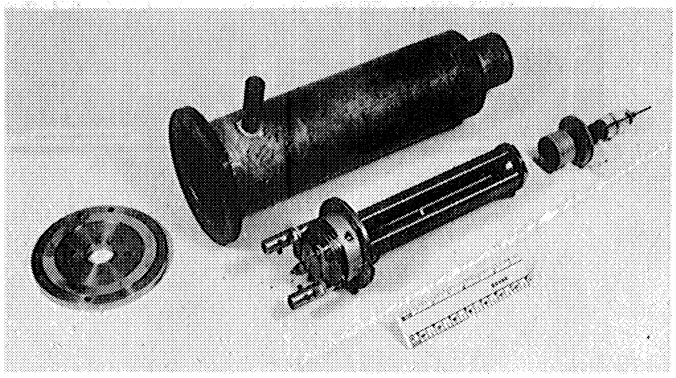

Figure A-3. Laboratory massenfilter.

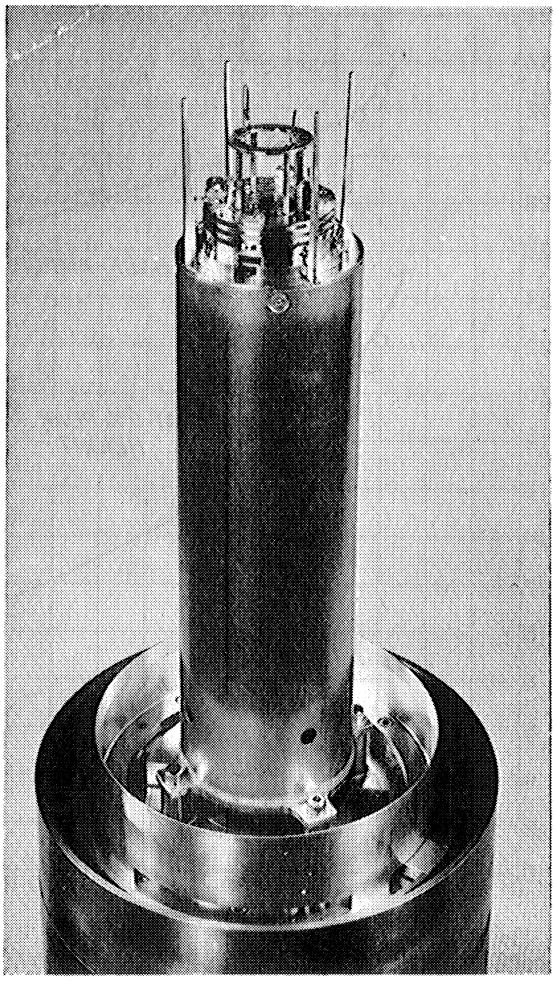

Figure A-4. Flight model.

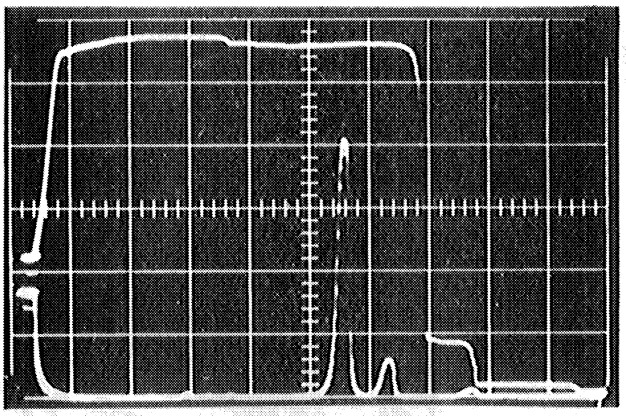

Figure A-5. Spectrum of air.

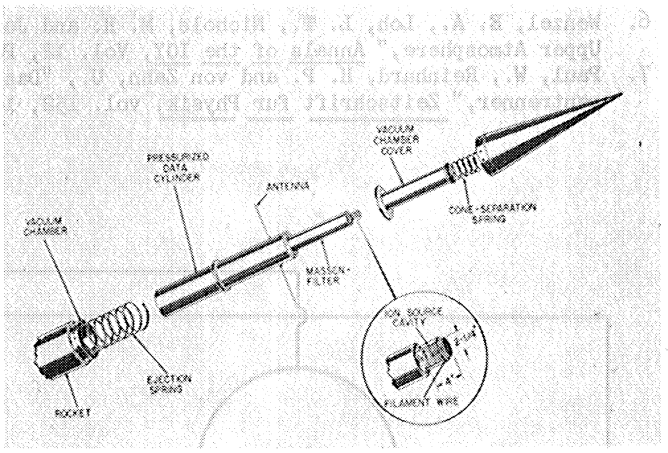

Figure A-7. Data cylinder separation.

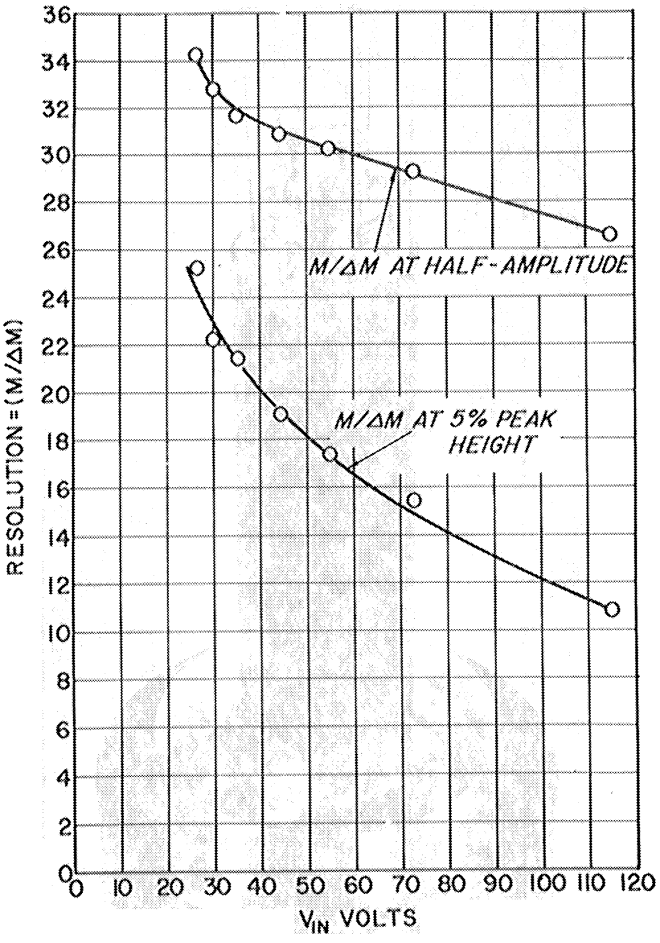

Figure A-6. Resolution of nitrogen as a function of injection voltage.

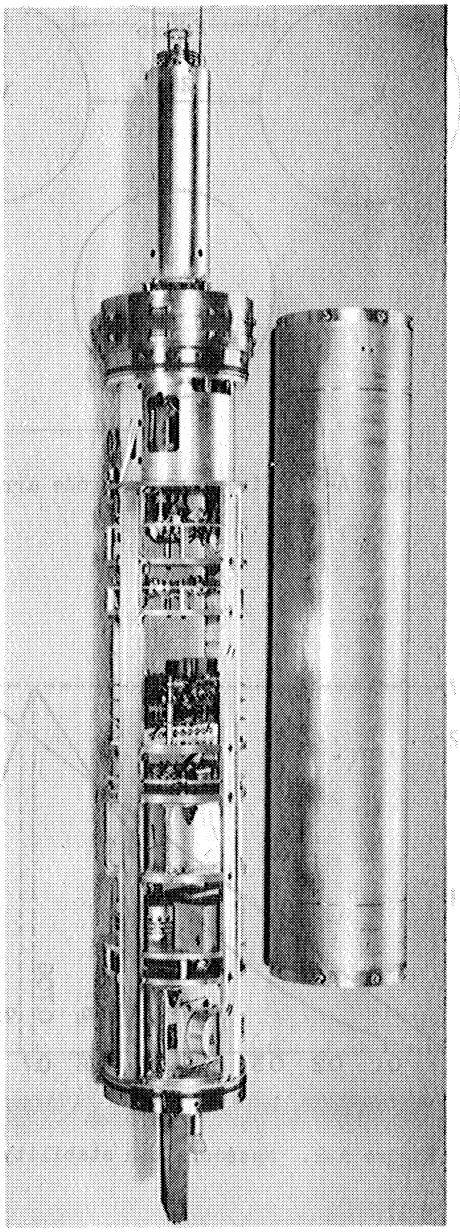

Figure A-8. Flight instrumentation.

APPENDIX B

MINOR CONSTITUENTS; NASA 10.91 UA

Throughout this section, the reader is cautioned that peak-peak noise on the telemeter channel was approximately 3×10^{-12} amp. Comments made throughout this section must therefore be regarded as tentative inasmuch as most of these constituents reach the noise level prior to apogee.

B.1 ATOMIC NITROGEN, N_1

Atomic nitrogen was apparent in both the conventional spectra and staircase spectra. The average value between 100 km and apogee lay between 0.02 and 0.04 of the N_2 ion current. Unfortunately, because of limitations due to electrometer noise and resolution at low mass numbers, no firm conclusions can be drawn from the results of this flight regarding possible dissociation of nitrogen except that N_1 probably exists at no greater concentration than 0.05 N_2. This is particularly true since the laboratory calibration data yielded a ratio of N_1/N_2 of 0.015, somewhat less than observed in flight, but not conclusive in the presence of noise.

B.2 WATER, H_2O

Figure B-1 shows the raw data points obtained from both staircase and conventional spectra for the mass 18 peak. The wide divergence between the staircase data and spectral peak data is undoubtedly due to the large kinetic cross-section of the water molecule. Here, again, the staircase mode yields the larger values due to the strong focusing action which overcomes the effects of scattering collisions to much higher densities than the conventional mode of operation. Since upleg and downleg data show many of the characteristics of the major constituents, the authors suspect that a substantial portion of the current was due to the ambient atmosphere. The rising currents with decreasing altitudes on the downleg, for example, cannot be explained on the basis of outgassing of the ion source alone. However data from future flights will be awaited before further work on this constituent will be undertaken.

B.3 MASS 44 AND RESIDUAL ION CURRENTS

The mass 44 spectral peak current is shown as a function of altitude in Fig. B-2. This peak may be due to CO_2 or N_2O both of which have a mass of 44 amu. The RF voltage at the end of the sweep was large enough to clearly show the mass 40 step in the staircase mode but was not sufficient to include the mass 44 step. Hence, the residual current (Fig. B-3) obtained from the staircase mode, includes the mass 44 ion current together with all constituents greater than mass 40.

Unfortunately, the mass 44 peak was too small to detect in the presence of noise except at the lower part of the trajectory. In the altitude range for which it is shown, however (Fig. B-2), it exhibits many of the characteristics of the major constituents. This suggests that a significant portion of the mass 44 peak is of ambient origin.

On the other hand, if one were to subtract the mass 44 ion current from the residual current of Fig. B-3, the remainder would be almost constant with altitude. This leads to the conclusion that the residual components above mass 44 are almost entirely due to constituents which emanated from the metal surfaces in the vicinity of the ion source.

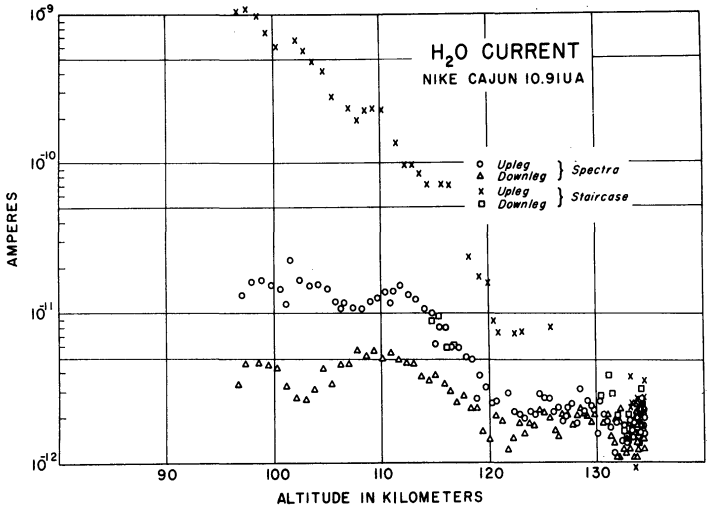

Fig. B-1. H_2O current.

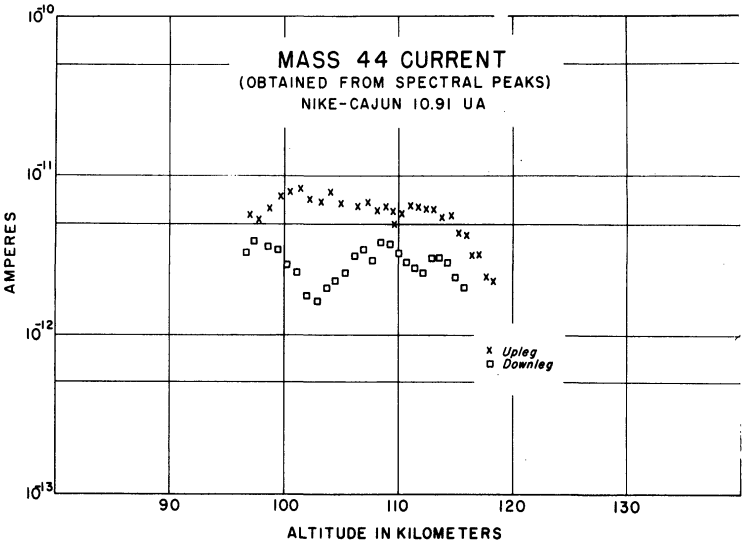

Fig. B-2. Mass 44 current.

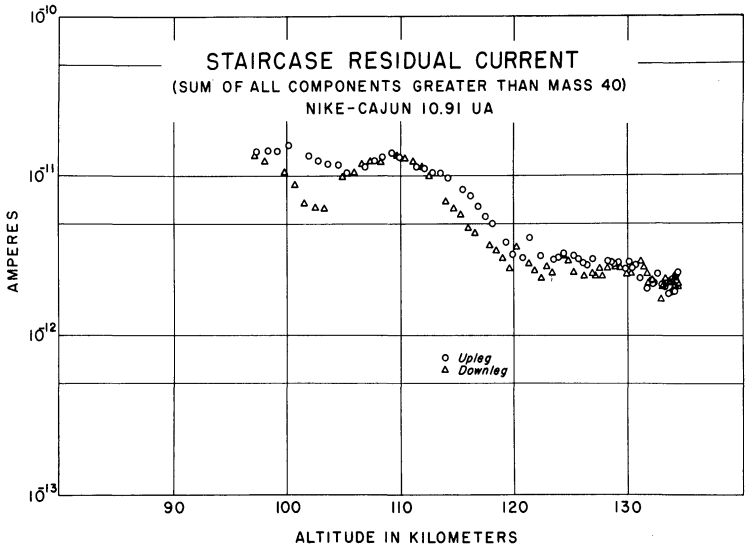

Fig. B-3. Staircase residual current.

APPENDIX C

RECOMBINATION EFFECTS IN EARLIER MEASUREMENTS

Earlier measurements of O_1/O_2 were made using Bennett tubes. The typical Bennett tube has many grids so that after an oxygen atom has entered the tube it may be expected to have many collisions with grids and walls before it finds its way back out. Although the grids are relatively transparent when viewed along the axis they become less so at angles relative to the axis, approaching opaqueness at 90°. Thus the grids have a sort of trapping effect which, among other things, can result in numerous passages in the ionizing region. This results in an increased probability of ionization relative to the incoming atom or molecule, which must be partially collimated in order to reach the ionizing region before interacting with the walls.* Assuming that the difference between our results and the earlier results is due to recombination in the apparatus, the following is an attempt to provide some insight into the phenomena.

A detailed analysis of a particular tube would be prohibitively complicated. However, some feel for the situation may be achieved by use of a simplified two-dimensional model. Let the Bennett tube be replaced by a cylinder with its axis in the x direction and consider motion in a plane including the x axis. Let the distance between the walls be unity. Let the angle of scattering from the walls be θ measured from the normal. Assume that the angle of scattering is independent of the angle of incidence. Let the probability density function of θ be

$$P(\theta) = (2/\pi)\cos^2\theta \qquad -90° < \theta < 90° \tag{C-1}$$

This function is rather mildly peaked at $\theta = 0$ to represent preponderance of scattering normal to the axis of the tube due to the grids, etc. The distance traveled along the axis of the cylinder between collisions with the walls is given by $\tan\theta$. From Eq. (C-1) the distribution function of $\tan\theta$ is

$$P(\tan\theta) = (2/\pi)\cos^4\theta = 2/\pi(1+x^2)^2 \tag{C-2}$$

where $x = \tan\theta$. The rms value, σ_x, of x is

$$\sigma_x = 1 \tag{C-3}$$

After N bounces, the mean of the sum of the individual x's is zero and the rms value σ_{Nx} is

$$\sigma_{Nx} = \sqrt{N} \tag{C-4}$$

If N is large, then by the central Limit Theorem it may be assumed that the distribution of the sum is approximately Gaussian. If N is 100, for example, then $\sigma_{Nx} = 10$. Then, assuming a Gaussian distribution, the probability, after 100 wall collisions, of traveling along the x axis a distance of ten diameters or more in one direction is 0.16.

In such a model, an oxygen atom, after entering the ionizing region of the Bennett tube, is very likely to experience many collisions with walls and grids before escaping from the tube. Experimental determinations of the probability of recombination of atomic oxygen upon collision with a metal under conditions similar to those encountered with a Bennett tube have been reported [C-3, C-4].

The results may be summarized in the following table:

Table C-1

Metal	Temperature	ρ_c	Authors	Date
Pt	200°C	0.010±0.002	Hacker, Marshall & Steinberg	1961
Pt	850°C	0.10 ±0.02	Hacker, Marshall & Steinberg	1961
Pt	380°K	0.001	Wood and Wise	1960
Al	364°K	0.017	Wood and Wise	1960
Pt	1100°K	0.004	Wood and Wise	1960

For purpose of illustration, Table C-2 shows the expected fraction, f_a, of atoms (i.e., fraction not recombined) left after 100 collisions with the surface as a function ρ_c, the probability of recombination per collision.

Table C-2

ρ_c	f_a
0.01	0.36
0.02	0.13
0.03	0.05

*In this respect, the authors disagree with Istomin [C-1] who assumes that the probability of ionization of the reverse flux is the same as the incident flux. Also, for the same reason, we disagree with Pokhunkov's method of estimating a correction for his Bennett tube data [C-2]. His corrected data for the O_1/N_2 number density ratio agree roughly with ours at 135 km even though his ion current ratio is approximately 1/8 of ours.

Thus with the typical Bennett tube, even with a very short inlet tube, it is reasonable to expect very substantial amounts of recombination prior to ionization. With the ion source used in the experiment reported in this paper, an atom can be expected to experience, on the average, only one to two surface collisions prior to its escape.

Wood and Wise [C-4] also reported experiments in the recombination of N upon collision with nickel and gold. The probability of recombination on nickel per collision is 0.1 independent of temperatures over the range $1000 > T > 350°K$ and on gold the value is 0.01 at 300°K and 0.1 at 1000°K. Thus one may expect recombination effects to be more severe with atomic nitrogen than with atomic oxygen.

REFERENCES

C-1. V. G. Istomin. Mass Spectrometric Measurements of Gas Composition of the Earth's Atmosphere by Means of Rockets and Satellites. Geomagnetism and Aeronomy, 1 (1963), 321-328.

C-2. A. A. Pokhunkov. On the Variation in the Mean Molecular Weight of Air in the Night Atmosphere at Altitudes of Loo to 210 km From Mass Spectrometer Measurements. Planet Space Sci. 11 (1963), 297-304. Trans. from Iskusstvennye Spntniki Zemli 12 (1962), 133.

C-3. D. S. Hacker, S. A. Marshall, and M. Steinberg. Recombination of Atomic Oxygen on Surfaces. J. Chem. Phys. 35 (1961), 1788-1792.

C-4. J. Wood and H. Wise. The Interaction of Atoms with Solid Surfaces, Rarefied Gas Dynamics. Academic Press, New York (1961), 51-59.

APPENDIX D

ANGLE OF PRECESSION

Assuming that the instrument package is symmetric about the longitudinal axis, the following equation can be used to determine the precession cone half-angle θ*

$$\dot{\phi} \cos \theta = \omega_3 (I_3/I_1) \qquad \text{(D-1)}$$

where: $\dot{\phi}$ = angular velocity of precession
θ = half angle of the precession cone
ω_3 = angular velocity component along longitudinal axis of package

The received field strength of the telemetry signal show a period of 1.2 sec which may be associated with ω_3. The ion current data show a period of 31 sec which may be associated with $\dot{\phi}$. The moment of inertia I_3 is about the longitudinal axis of the package and I_1 is the moment of inertia about an axis perpendicular to the longitudinal axis. Both pass through the CG.

The moments of inertia I_3 and I_1 were not measured prior to the flight of NASA 10.91 UA and we have no duplicate package. Therefore, these moments are calculated approximately from our knowledge of the package geometry. Actually, the package was not exactly symmetric. However, assuming that it was symmetric, the calculated ratio I_3/I_1 is 0.028. Substitution into Eq. (D-1) gives

$$\theta = \cos^{-1} 0.72 = 44° \qquad \text{(D-2)}$$

Since the ratio of I_3/I_1 is only approximate and may be expected to be subject to error of ±10% or so, θ may be expected to lie between 40° and 50°. This provides a qualitative explanation of the ion current versus altitude curves.

*See, for example, J. C. Slater and N. H. Frank, Mechanics, p. 112, Eq. (3.4), McGraw-Hill Book Co., New York (1947).